A preliminary exploration of the mechanism for the occurrence of two types of various magnetic structures in the magnetotail

JIN Shuping[1], HU Xianpeng[1], CUI Hailong[1], LIU Zhenxing[2], PU Zuyin[3] & B. Wilken[4]

1. Department of Earth and Space Science, University of Science and Technology of China, Hefei 230026, China;
2. Center for Space Sciences and Application Research, Chinese Academy of Sciences, Beijing 100080, China;
3. Department of Geophysics, Peking University, Beijing 100871, China;
4. Max-Planck Institut fuer Aeronomie, D-37191 Katlanburg-Lindau, Germany

Abstract **As well known, the magnetic cross-tail component B_y in the magnetotail is in direct proportion to the interplanetary magnetic field (IMF) B_y component. And the polarity of IMF and plasmoid / flux rope B_y components do indeed agree. This results indicate that the IMF B_y penetrates plasmoids and the magnetic structures must therefore be three-dimensional. In this note, the dynamical processes of magnetotail in the course of a substorm are studied using a MHD code with two-dimensions and three components on the basis of two types of initial equilibrium solutions of the quiet magnetotail. The numerical results of two cases illustrate various features of time evolution of B_y component that correspond to two kinds of plasmoid-like structures: one is associated with a flux rope core and the other resembles a "closed loop" plamoid. Therefore, the occurrence of various magnetic structures in the magnetotail might be related to nonsteady driven reconnection with different distributions of the B_y component.**

Keywords: magnetospheric substorm, magnetic cross-tail component B_y, plasmoid-like structures, nonsteady magnetic reconnection.

Observations of magnetic structures in the magnetotail have frequently shown bipolar perturbations in the B_z component of the magnetic field. These are thought to be

(*Continued from page* 980)

7. Sun, D. H., Shaw, J., An, Z. S. et al., Matuyama/Brunhes transition recorded in Chinese loess, J. Geomag. Geoelectr., 1993, 45: 319.
8. Zheng, H. B., Rolph, T. C., Shaw, J. et al., A detailed palaeomagnetic record for the last interglacial period, Earth Planet. Sci. Lett., 1995, 133: 339.
9. Fang, X. M., Li, J. J., van der Voo, R. et al., A record of the Blake Event during the last interglacial paleosol in the western Loess Plateau of China, Earth Planet. Sci. Lett., 1997, 146: 73.
10. Guo, B., Zhu, R. X., Yue, L. P. et al., Cobb Mountain event recorded in the Chinese loess, Sci. in China, Ser. D, (in Chinese), 1998, 28(4): 327.
11. Guo, B., Zhu, R. X., Ding, Z. L. et al., Upper Jaramillo polarity transition and short geomagnetic event recorded in a loess section at Jingbian, northern China, Chinese Sci. Bull., 1999, 44: 1907.
12. Rolph, T. C., The Matuyama-Jaramillo R-N transition recorded in a loess section near Lanzhou, P. R. China, J. Geomag. Geoelectr., 1993, 45: 301.
13. McIntosh, G., Rolph, T. C., Shaw, J. et al., A detailed record of normal-reversed-polarity transition obtained from a thick loess sequence at Jiuzhoutai, near Lanzhou, China, Geophys. J. Int., 1996, 127: 651.
14. Zhu, R. X., Guo, B., Ding, Z. L. et al., Gauss-Matuyama polarity transition obtained from a loess section at Weinan, north-central China, Chinese J. Geophy. (in Chinese), 2000, 43(5): 635.
15. Zhou, L. P., Shackleton, N. J., Misleading positions of geomagnetic reversal boundaries in Eurasian loess and implications for correlation between continental and marine sedimentary sequences, Earth Planet. Sci. Lett., 1999, 168: 117.
16. Heller, F., Evans, M. E., Loess magnetism, Rev. Geophys., 1995, 33: 211.
17. An, Z. S., Ho, C. K., New magnetostratigraphic dates of Lantian Homo erectus, Quat. Res., 1989, 32: 213.
18. Zheng, H. B., An, Z. S., Shaw, J., New contributions to Chinese Plio-Pleistocene magnetostratigraphy, Phys. Earth Planet. Inter., 1992, 70: 146.
19. Stacey, F. D., Banerjee, S. K., The Physical Principles of Rock Magnetizm, New York, Elsevier, 1974, 124—145.
20. Florindo, F., Zhu, R. X., Guo, B. et al., Magnetic proxy climate results from the Duanjiapo loess section, southernmost extremity of the Chinese Loess Plateau, J. Geophys. Res., 1999, 104: 645.
21. Day, R., Fuller, M., Schmidt, V. A., Hysteresis properties of titanomagnetites: grain-size and compositional dependence, Phys. Earth Planet. Int., 1977, 13: 260.
22. Zhu, R. X., Wu, H. N., Li, C. J. et al., Magnetic property of Chinese loess and its paleoclimate significance, Sci. in China, 1995, 38(2): 238.
23. Ding, Z. L., Yu, Z. W., Rutter, N. W. et al., Towards an orbital time scale for Chinese loess deposits, Quart. Sci. Rev., 1994, 13: 39.
24. Kukla, G., Heller, F., Liu, X. M. et al., Pleistocene climates in China dated by magnetic susceptibility, Geology, 1988, 16: 811.
25. Jacobs, J. A., Reversals of the Earth's Magnetic Field, New York: Cambridge Univ., 1994, 69—125.
26. Meeril, R., McElhinny, M., McFadden, P., The Magnetic Field of the Earth: Paleomagnetism, the Core, and the Deep Mantle, San Diego: Academic Press, 1996, 98—203.
27. Zhou, L. P., Oldfield, F., Wintle, A. G. et al., Partly pedogenic origin of magnetic variations in Chinese loess, Nature, 1990, 346: 737.
28. Hunt, C. P., Singer, M. L., Kletetschka, G. et al., Effect of citrate-bicarbonate-dithionite treatment on fine-grained magnetite and maghemite, Earth Planet. Sci. Lett., 1995, 130: 87.
29. Zhu, R. X., Lin, M., Pan, Y. X., History of the temperature-dependence of susceptibility and its implications: Preliminary results along an E-W transect of the Chinese Loess Plateau, Chinese Sci. Bull., 1999, 44(supp): 81.
30. Deng, C. L., Zhu, R. X., Verosub, K. L. et al., Paleoclimatic significance of the temperature-dependent susceptibility of Holocene loess along a NW-SE transect in the Chinese loess plateau, Geophy. Res. Lett., 2000, 27: 3715.
31. Lu, J. Z., Xu, X. H., Wen, D. Y., Analyzing of the climatic variation factors such as annual precipitation and annual average temperature in Lantian county, the northern hillside of Qinglin Mountains, Shaanxi Materology (in Chinese), 1998(5): 14.
32. Liu, Y. F., Yu, X., Xu, X. H. et al., Research on the source of the natural falling water in Xi'an, Shaanxi Meterology (in Chinese), 1998(4): 12.

(Received November 30, 2000)

created by reconnection processes. In addition, the existence of significant B_y component across the tail, which is proportional to the IMF B_y, is a well-known fact[1, 2]. Based on magnetic field measurements over a large faction of the magnetotail, an approximate expression B_y (magnetotail) ~ 0.13 B_y (IMF) was found[1]. Moreover, a comparison of B_y observations within plasmoids with simultaneous upstream IMF B_y data[3] indicates that the polarity of the IMF B_y is in agreement with that in the plasmoid. Consequently, a plasmoid should be considered as a three-dimensional structure. Five plasmoid-like structures associated with five energetic ion bursts were identified by Geotail observations in the deep tail ($x = -96R_E$) during an isolated substorm on January 15, 1994. Ref. [4] shows Geotail particle and magnetic field data, in which the five plasmoid events are marked P_1 to P_5. Ref. [4] indicates that in the P_2 event the B_y and B_z components show bipolar signatures; but in the third event P_3 the bipolar waveforms can be observed only in the B_z component and in coincidence with the inflection point of the B_z bipolar signatures, the B_y component shows a peak value. However, the P_1, P_4 and P_5 events do not show any indication for bipolar signatures in the B_z component.

In this note, taking aim at an exploration of the mechanism for the occurrence of various magnetic structures, MHD equations are numerically resolved. The simulation space is in rectangular plane (x, z), in which the x coordinate is in the anti-earth direction, the z coordinate is perpendicular (northward) to the plasmoid sheet, and the y coordinate is consistent with a right-handed coordinate system of x and z. A magnetic flux function $A(t, x, z)$ being related to the magnetic field is introduced by the equation

$$\boldsymbol{B} = \nabla \times (A\,\boldsymbol{e}_y) + B_y \boldsymbol{e}_y. \tag{1}$$

The MHD equations of two-dimension and three-component including the resistivity are written in a dimensionless form:

$$\frac{\partial \rho}{\partial t} + \nabla \cdot (\rho\, \boldsymbol{v}) = 0, \tag{2}$$

$$\frac{\partial \boldsymbol{v}}{\partial t} + \boldsymbol{v} \cdot \nabla \boldsymbol{v} + \frac{1}{\rho} \nabla \left(\rho T + \frac{F}{2} B_y^2 \right) + \frac{F}{\rho} \Delta A \nabla A + \frac{F}{\rho} \nabla A \times \nabla B_y = 0, \tag{3}$$

$$\frac{\partial A}{\partial t} + \boldsymbol{v} \cdot \nabla A - \chi_{\mathrm{m}} \Delta A = 0, \tag{4}$$

$$\frac{\partial B_y}{\partial t} + \nabla \cdot (B_y \boldsymbol{v}) - (\nabla \boldsymbol{v}_y \times \nabla A) \cdot \boldsymbol{e}_y - \chi_{\mathrm{m}} \Delta B_y = 0, \tag{5}$$

$$\frac{\partial T}{\partial t} + \boldsymbol{v} \cdot \nabla T + (\gamma - 1) T\, \nabla \cdot \boldsymbol{v} = 0, \tag{6}$$

where

$$\chi_{\mathrm{m}} = \frac{\eta_{\mathrm{m}}}{v_0 l_0}, \quad F = \frac{A_0^2}{\rho_0 l_0^2 v_0^2}, \quad v_0 = \sqrt{RT_0}. \tag{7}$$

The length, magnetic field strength, density, temperature, magnetic flux function and velocity are expressed in units of l_0 (= L_z =20R_E, the half-length of simulation box in the z direction), B_∞ (the initial value of B_x at $x = 0,\ z = L_z$), ρ_∞ (the initial plasma density on the boundary of magnetotail $z = L_z$), T_0 (the initial temperature), $A_0 = B_\infty l_0$, $v_0 = \sqrt{RT_0}$ (R is the gas constant), respectively.

The magnetic Reynolds number is given by

$$R_{\mathrm{m}} = \frac{V_{\mathrm{A}} l_0}{\eta_{\mathrm{m}}} = \frac{V_{\mathrm{A}}}{\chi_{\mathrm{m}} v_0}, \tag{8}$$

where η_{m} is the resistivity (or magnetic viscosity), $V_{\mathrm{A}} = B_{\mathrm{c}} / \sqrt{4\pi \rho_\infty}$ is the Alfven speed with B_{c} which is the initial magnetic field at $x = 100R_E, z = l_0 = 20R_E$ and related to B_∞ by $B_{\mathrm{c}} = 0.5780\, B_\infty = 10nT$. In the present study, the resistivity η_{m} is assumed to be uniform and magnetic Reynolds number is set as: $R_{\mathrm{m}} = 4624$.

We assume the magnetotail to be initially in a static equilibrium state. The equations for $B_y(x,z)$, $P(x,z)$ and $A(x,z)$ can be determined by the equilibrium solution as follows:

$$B_y(x,z) = B_y(A), \quad P(x,z) = P(A),$$

and

$$\nabla^2 A = -4\pi \frac{\mathrm{d}P^*(A)}{\mathrm{d}\,A}, \tag{9}$$

where $P^*(A) = P(A) + \frac{B_y^2(A)}{8\pi}$. Assuming $A(x,\ z)$ week variations with respect to x, the magnetic flux function can be obtained from eq. (9):

$$A(x,z) = B_\infty L_{\mathrm{c}} \left[\ln\cosh\left(\frac{H(x) z}{L_{\mathrm{c}}} \right) - \ln H(x) \right], \tag{10}$$

where $H(x)$ varies slightly in x and is expressed by

$$H(x) = \left(1.0 + \frac{bx}{\nu L_{\mathrm{c}}} \right)^{-\nu}, \tag{11}$$

where we set $b = 0.018, \nu = 0.6, L_{\mathrm{c}} = 0.1 l_0 = 2R_E$.

For the uniform initial temperature T_0, by using eqs. (9) and (10), two types of $B_y(x,z)$ and $\rho(x,z)$ which are satisfied for the equilibrium condition are given by the following expressions.

Type Ⅰ.

$$= 2nT\ , \quad \frac{\mathrm{d}}{\mathrm{d}A}\left(\frac{B_y^2}{8\pi}\right) = 0, \tag{12}$$

$$\rho(x,z) = \rho_\infty + \rho_{\mathrm{c}}\left[\frac{H(x)}{\cosh(\frac{H(x)z}{L_{\mathrm{c}}})}\right]^2. \tag{13}$$

Thus, at $x = 0$ and $z = 0$ the density is $\rho(0,0) = \rho_\infty + \rho_{\mathrm{c}}$, here $\rho_{\mathrm{c}} = \frac{B_\infty^2}{8\pi RT_0}$.

Type Ⅱ.

$$B_y(x,z) = \sqrt{(1-\alpha)}B_\infty \frac{H(x)}{\cosh\left(\frac{H(x)z}{L_{\mathrm{c}}}\right)}, \tag{14}$$

$$\rho(x,z) = \rho_\infty + \alpha\rho_{\mathrm{c}}\left[\frac{H(x)}{\cosh\left(\frac{H(x)z}{L_{\mathrm{c}}}\right)}\right]^2, \tag{15}$$

where α is a constant with values $0 < \alpha \leqslant 1$. It can be found by comparing eqs. (12) and (13) with eqs. (14) and (15) that the distribution of B_y in type Ⅱ is significantly different from that in type Ⅰ, but the distribution of the plasma density in type Ⅱ is similar to that in type Ⅰ. It can also be seen from eqs. (14) and (15) that ρ increases and B_y decreases with α increasing and $B_y = 0$ when $a = 1.0$. In this study, the case with $a = 0.9$ is investigated. We take $T_0 = 1.66\times10^6$ K, $\rho_\infty = 1.67\times10^{-25}$ g/cm^3 (corresponding to $n_{\mathrm{ion}} = 0.1$ proton /cm^3), $B_\infty = 17.3nT$, hence $\rho_{\mathrm{c}} = 4.34\times10^{-24}$g/cm^3 (corresponding to $n_{\mathrm{ion}} = 2.6$ proton/cm^3), $B_{\mathrm{c}} = 10\ nT$, the Alfven velocity $V_{\mathrm{A}} = B_{\mathrm{c}} / \sqrt{4\pi\rho_\infty} = 690.3$ km/s, and the characteristic time is then given by $\tau_{\mathrm{A}} = l_0/V_{\mathrm{A}} = 184.6$s. The respective system is then assumed to be initially in a static isothermal state, that is, $v_x = v_y = v_z = 0$ and $T = T_0$. Two types of equilibrium solutions of a quiet magnetotail are used as the initial states of the simulation study. The lengths of the simulation box in the z direction and in the x direction are taken to be $L_z = 20R_E$ and $L_x = 110R_E$ (the unit of length is set as $l_0 = L_z$). The simulation is carried out in the upper half plane, i.e. the computational domain is taken to be $0\leqslant x\leqslant L_x$, $0\leqslant z\leqslant L_z$, since the symmetric boundary conditions are imposed at the bottom boundary ($z = 0$). The computational domains $0\leqslant x\leqslant L_x$, $0\leqslant z\leqslant L_z$ are divided into 23×56 grid points. In order to allow adequate spatial resolution in the neutral sheet of magnetotail, the grid spacing in the z direction increases according to a geometric series and a uniform mesh is adopted in the x direction.

We assume that a dawn-dusk electric field E is imposed on the boundary of magnetotail. Along the top boundary the electric field E is uniform in the range of $100R_{\mathrm{E}}\leqslant x\leqslant 110R_E$ and E decreases linearly to zero within $0\leqslant x\leqslant 100R_E$. Thus, an inward plasma flow $v_z = -cEB_x/B^2$, $v_x = -cEB_z/B^2$ is formed along the top boundary under the interaction of the electric field E and magnetic field B. The driven plasma inflow leads to the intermittent occurrence of the multiple X-line reconnection. The numerical results of all the two cases illustrate the repeated formation and progressive emission of the plasmoids with high density and high temperature. This means that a large amount of energy stored in the magnetotail is gradually dissipated by ejecting multiple plasmoids in the course of strong substorms. These results are in line with the features of multiple-plasmoid-like structures observed on Jan. 15, 1994 with Geotail. In this observation, five plasmoids are associated with five quasi-periodic energetic ion bursts. The repeated feature reproduced in this work is similar to that in the simulations with two-dimensions and two-components, more details can be found in refs. [5] and [6]. In the present study, two types of equilibrium solutions are used as the initial state of the simulation. Taking the different time evolution of B_y component into account, two kinds of plasmoid-like structures will be discussed.

Type Ⅰ. At $t = 0$, $A(x,z)$, $B_y(x,z)$ and $\rho(x,z)$ are expressed by eqs. (10), (12) and (13), respectively. We set the electric field $E=0.08$ which is in unit of $E_0 = V_{\mathrm{A}}B_\infty / c$. The time variations of the total magnetic field amplitude B and three components B_x, B_y and B_z at the point ($x = 70R_E$, $z = -0.3R_E$) are shown in fig. 1. The bipolar signatures in the B_z component appear when a plasmoid passes this point in the neutral sheet. As shown in fig. 1 at $t\approx 49\tau_{\mathrm{A}}$, $65\tau_{\mathrm{A}}$, $73\tau_{\mathrm{A}}$, $79\tau_{\mathrm{A}}$, $83\tau_{\mathrm{A}}$, $92\tau_{\mathrm{A}}$, $106\tau_{\mathrm{A}}$ and $112\tau_{\mathrm{A}}$, obvious (+ / –) bipolar signature in the B_z component can be observed. In coincidence with the inflection point of the B_z bipolar signatures, the B_y component shows a peak value, whereas the B_x component shows a depressed value and the field magnitude B is between a peak and a minimum value. The maximum B_y value in the plasmoid's center is about twice of the value outside the plasmoid region. Such an intense axial field at the structure's center represents an important feature of the plasmoid-like structure with a flux rope core. For the case of type Ⅰ, the distributions of B_y component in the

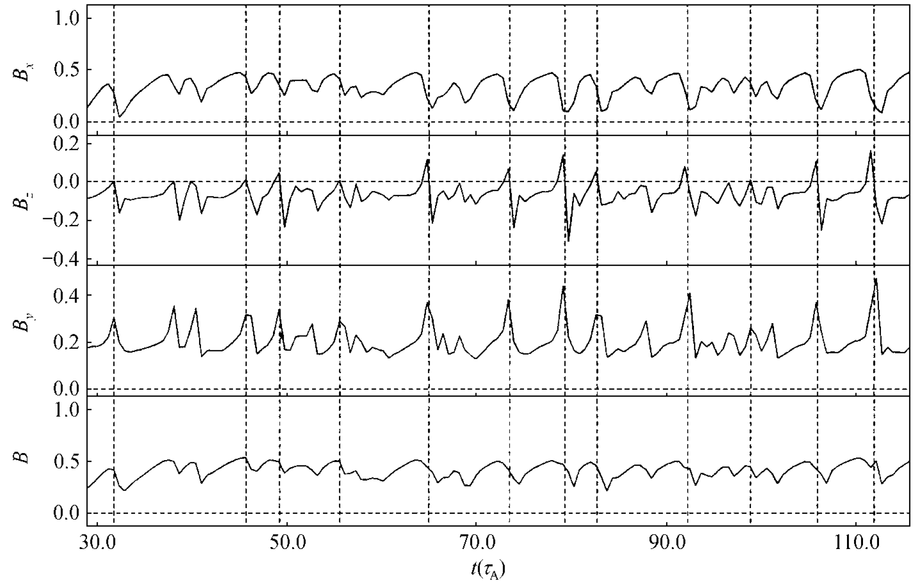

Fig. 1. Time history of magnetic field B($B=\sqrt{B_x^2+B_y^2+B_z^2}$) and three components B_x, B_y and B_z at a given point (x=70R_E, z =– 0.3 R_E) in the neutral sheet for the case of type Ⅰ.

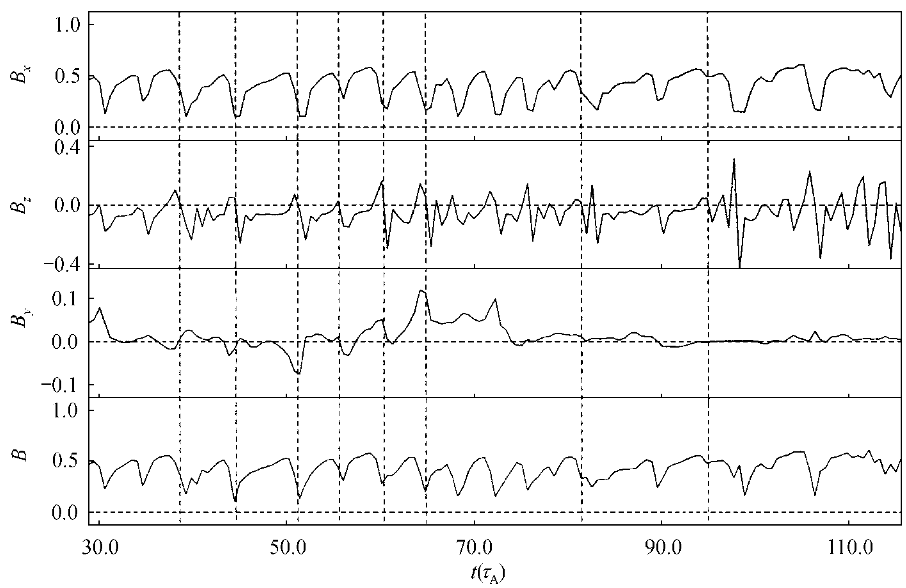

Fig. 2. Time history of the magnetic field B ($B=\sqrt{B_x^2+B_y^2+B_z^2}$) and three components B_x, B_y and B_z at a given point (x=70R_E, z = – 0.3R_E) in the neutral sheet for the case of type Ⅱ.

(x, z) plane are shown in fig. 2 at four different times. As shown in fig. 2, all B_y values are greater than zero and multiple B_y peak values exist in the plasma sheet. It can be found by comparing fig. 2 with the configuration of magnetic field lines (it is not displayed in this note) that the peak with the largest scale in the x-z direction always corresponds to the center of a pladmoid in the (x, z) plane. For example, at t =17.3τ_A, 67.1τ_A, 80.9τ_A and 94.8τ_A, the B_y peak located at x~40 R_E, 95 R_E, 90 R_E and 100R_E is in line with the plasmoid locations at the same time, respectively. This also indicates that for the case of type Ⅰ, the plasmoid structures always have a flux ropecore configuration displayed in fig. 1. It can be found by comparing the Geotail observation in ref. [4] with that in fig. 1 that the numerical result of type Ⅰ is similar to the main features of the P_3 plasmoid event in ref. [4]. In other words, the plasmoid-like structures with a flux rope core observed by Geotail can be reproduced by the case of type Ⅰ.

Type Ⅱ. At $t=0$, $A(x,z), B_y(x,z)$ and $\rho(x,z)$ are expressed by eqs. (10), (14) and (15), respectively. We set $\alpha = 0.9$, $E = 0.12$. The time variations of the total magnetic field amplitude B and three components B_x, B_y, B_z at the point ($x = 70R_E$,) are shown in fig. 3. The bipolar signatures in the B_z component are similar to those in fig. 1. This means that multiple plasmoids progressively pass through the neutral sheet of magnetotail. As shown in fig. 3, at the time when the bipolar signature passes through the inflection point, both and the total field B show relative minimum. This is a common characteristic of a "classic" plasmoid. However, in fig. 3 the time variation of the component shows a complex pattern. Most of the inflection points of the B_z (at about $39\tau_A$, $44.5\tau_A$, $51.5\tau_A$, $55.5\tau_A$ and $60\tau_A$) are accompanied with a B_y bipolar signature. Also, there are components with rather large values (for example, at $t = 65\tau_A$ and $72\tau_A$). By comparing fig. 3 with ref. [4] for the case of type Ⅱ, the kind of a plasmoid with bipolar signatures in the and components is similar to the features of P_2 plasmoid event.

The distributions of component in the (x, z) plane are given in fig. 4. As shown in the figure, at $t = 40.5\tau_A$, the component has generally negative values, but at $t = 66\tau_A$ and $75\tau_A$, the B_y component assumes positive values. However, later (e.g. $t = 107.5\tau_A$), the component changes again into negative values in a quite large area. Thus it can be concluded that, as time elapses, the sign of reverses if the reconnection process is still active. Furthermore, it can be found by comparing fig. 4 with the configuration of magnetic field lines (it is not displayed in this note) that the inflection regions of B_y component in fig. 4 appear to be near the plasmoid zones. Namely, for case of type Ⅱ, both and components show bipolar

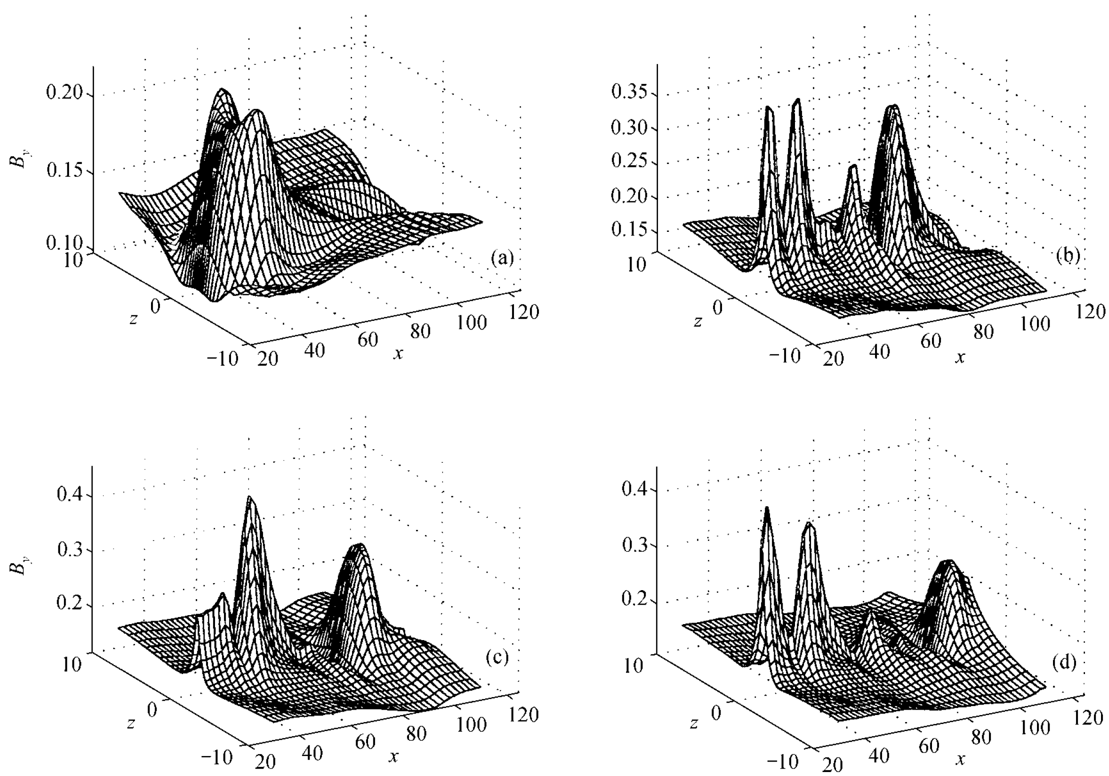

Fig. 3. The surface plot of B_y component of the magnetic field at different time for the case of type Ⅰ. (a) $t = 17.3\ \tau_A$; (b) $t = 65.9\ \tau_A$; (c) $t = 80.9\ \tau_A$; (d) $t = 94.8\ \tau_A$.

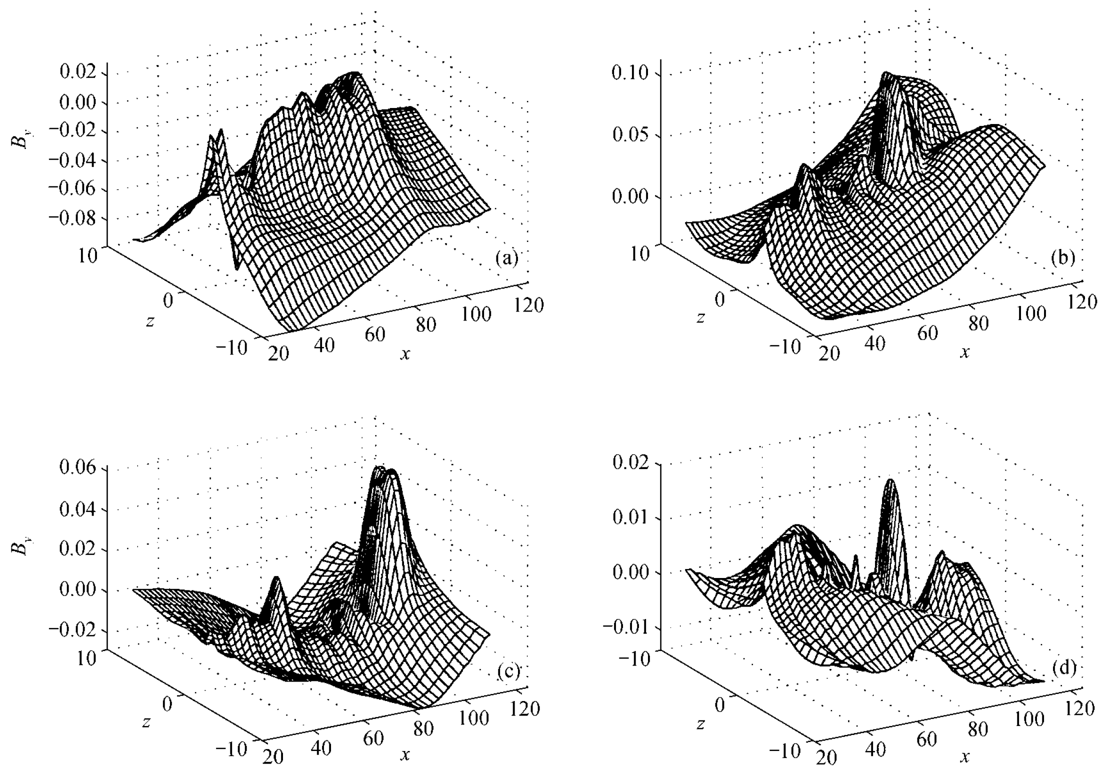

Fig. 4. The surface plot of B_y component of the magnetic field at different time for the case of type Ⅱ. (a) $t = 40.5\tau_A$; (b) t=65.9 τ_A; (c) t=74.6 τ_A; (d) t=107.5 τ_A.

signatures in some plasmoid regions. This is in agreement with the features displayed in $B_y \sim t$ and $B_z \sim t$ curves of fig. 3. Therefore, in ref. [4], the main features of P_2 event are reproduced by the simulation results of type Ⅱ. Perhaps, the magnetic field of this configuration resembles a "close loop" plasmoid with a symmetry axis roughly in the (y, z) plane, which forms an angle of approximately 45° with respect to the z axis. The inflection points of B_y and B_z bipolar waveforms are not in coincidence. This phase relation can result from the fact that the center of the plasmoid-like structure does not pass through the selected point in the neutral sheet ($x = 70R_E$, $z = -0.3\ R_E$).

In summary, a significant magnetic field B_y component in the magnetotail is closely correlated with the IMF and large B_y variations tend to be found during substorms[2]. As shown in the simulation, two kinds of plasmoid-like structures are associated with two types of B_y initial distributions. Therefore, the occurrence of various magnetic structures in the magnetotail might be related to the non-stationary driven reconnection with different distributions of the B_y component as found here.

Acknowledgements This work was supported by the National Natural Science Foundation of China (Grant Nos. 49874035 and 49834040) and the Space Physics Fund of the First-rate University Program.

References

1. Fairfield, D. H., On the average configuration of the geomagnetic tail, J. Geophys. Res., 1979, 84: 1950.
2. Lui, A. T. Y., Characteristics of the cross-tail current in the earth's magnetotail, in Geophysical Monograph 28 (ed. Potemra, T. A.), Washington D C: AGU Publishers, 1984, 158—170.
3. Hughes, W. J., Sibeck, D., On the 3-dimensional structure of plasmiods, Geophys. Res. Lett., 1987, 14: 636.
4. Zong, Q. G., Wilken, B., Reeves, G. et al., Geotail observation of energetic ion specics and magnetic field in plasmoid-like structures in the course of an isolated substorm event, J. Geophys. Res., 1997, 102(11): 409.
5. Jin, S. P., Ma, N., Liu, Z. X. et al., A simulation study of multiple plasmoids in the magnetotail during substorm event, Part Ⅰ, Acta Geophysica Sinica, 1997, 40(6): 727.
6. Jin, S. P., Ma, N., Hu, X. P. et al., A simulation study of multiple plasmoids in the magnetotail during substorm event, Part Ⅱ, Acta Geophysica Sinica, 1998, 41(5): 609.

(Received October 12, 2000)